SSRG International Journal of Electrical and Electronics Engineering
ISSN: 2348-8379/ https://doi.org/10.14445/23488379/IJEEE-V10I8P123

Volume 10 Issue 8, 235-242, August 2023

Original Article

Backstepping Sliding Mode Controller for Switched Reluctance Motor with Combined Nonlinear Model

Nha Phi Hoang[1], Hung Pham Van[2], Hai Le Xuan[3]

[1,2]*Ha Noi University of Industry, Ha Noi, Vietnam.*
[3]*VNU International School, Ha Noi, Vietnam.*

[2]*Corresponding Author : phamvanhung@haui.edu.vn*

Received: 24 June 2023 Revised: 27 July 2023 Accepted: 18 August 2023 Published: 31 August 2023

Abstract - *Today, Switched Reluctance Motors (SRM) are widely used in research and daily life due to their ability to provide large starting torque and low manufacturing costs. In terms of kinematics and control, the SRM drive system displays high nonlinearity due to the motor structure and the nonlinearity of the inverter, which switches between phases to operate the motor. Most current research focuses on controlling the SRM without considering the nonlinearity caused by the inverter. A few studies have dealt with controlling combined systems consisting of SRM and the inverter by linearizing the SRM model. Although this method is simple, the control quality is not high as it fails to account for the nonlinearity of the model. This paper presents a nonlinear control algorithm for the combined model of the switched reluctance motor and the Inverter, specifically the backstepping sliding mode control algorithm, which ensures the asymptotic stability of the system according to the Lyapunov standard. The simulation results demonstrate that the controller synthesized from the combined nonlinear model provides good control quality compared to the previously published H infinity nonlinear feedback controller, particularly when it comes to responding to changes in the speed setpoint and effectively handling load disturbances.*

Keywords - *Asymptotic stability, Backstepping sliding mode control, Speed control, SRM, Switched reluctance motor.*

1. Introduction

The Switched Reluctance Motors (SRM) have many advantages, such as a large starting torque, simple structure, low manufacturing cost, and high stable working ability [1-4]. Due to these benefits, switched reluctance motors have gradually been applied more widely recently, especially in the field of electric vehicles for tourism. However, this type of motor also exhibits certain disadvantages, such as significant pulsating torque, challenging control requirements, and high nonlinear characteristics. The strong nonlinearity in the SRM is primarily due to its inherent structure, further amplified by the presence of a phase-switching inverter, which contributes to increased resonance nonlinearity.

Consequently, it is crucial not to overlook the impact of the nonlinearity in the SRM's kinematics caused by the simultaneous excitation of the stator phases. Addressing this nonlinearity becomes a significant challenge that must be tackled [5-9]. Although some studies have provided a mathematical model of SRM [10-19], most of them have stopped at the motor's own mathematical model, ignoring the nonlinearity produced by the inverter. The author group Rigatos initially published a mathematical model of the SRM [20], which encompasses both the motor and the switch (Inverter). However, they modeled the SRM as a linear model to design an H-infinity nonlinear feedback controller, resulting in an incomplete consideration of the nonlinearity. Moreover, the control quality, such as large overshoot and long settling, must be improved. Inheriting research [20], the authors of this paper maintain the combined nonlinear model of the switched reluctance motor and then apply a nonlinear control algorithm to improve the quality of the drive system's switched reluctance mechanism.

Some published works, such as [21-27], have used the Backstepping nonlinear algorithm for the nonlinear model incorporating SRM. However, it has been found that the remaining disadvantage of the Backstepping control algorithm is the slow response speed, especially when the system is affected by noise, such as load disturbance. Therefore, in this paper, the authors use the backstepping sliding mode control algorithm to improve this problem. After the general introduction, the paper presents the mathematical model of SRM, which is a combination of both the motor and the Inverter in Part 2. Part 3 presents the backstepping sliding mode control algorithm for SRM. Part 4 presents the simulation results compared with the speed response using the backstepping algorithm. Finally, the paper concludes.

2. Combined Model of the Switched Reluctance Motor

The mathematical model of a 4-phase switched reluctance motor (Figure 1), according to the document [20], includes the following equations.

$$\begin{cases} \dfrac{d\theta}{dt} = \omega \\ \dfrac{d\omega}{dt} = \dfrac{1}{J}\left\{\sum_{j=1}^{4} T_j(\theta, i_j) - T_l(\theta, \omega)\right\} \\ \dfrac{di_j}{dt} = -\left(\dfrac{\partial \psi_j}{\partial i_j}\right)^{-1}\left(Ri_j + \dfrac{\partial \psi_j}{\partial \theta}\omega\right) + \left(\dfrac{\partial \psi_j}{\partial i_j}\right)^{-1} u_j \end{cases} \quad (1)$$

within j = 1, 2, 3, 4 (consider with 4 phases switched reluctance motor). In Equation (1), u_j, R and i_j are respectively the voltage, resistance and current of jth phase, θ is the rotor angular and ψ_j is the flux of phase j, T_j is the torque of phase j, the load torque T_l, the moment of inertia J and the single-phase torque in the SRM.

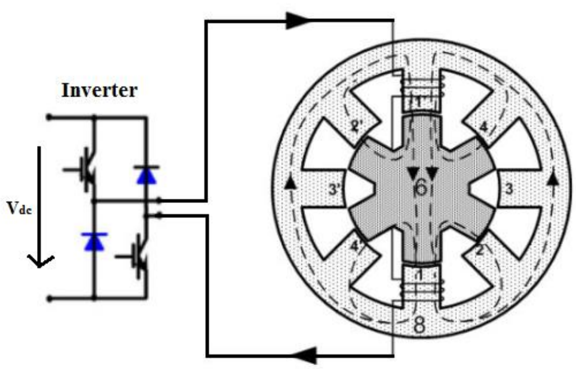

Fig. 1 SRM 8/6 and its control circuit (inverter)

According to [20], the magnetic flux characteristic of a 4-phase switched reluctance motor can be expressed as follows,

$$\psi_j(\theta, i_j) = \psi_s(1 - e^{-i_j f_j(\theta)}) \quad (2)$$

Where j = 1, 2, 3, 4, ψ_s is the saturation flux, N_r is the number of rotor poles, and the function $f_j(\theta)$ in Equation (3)

$$f_j(\theta) = a + b\sin[N_r\theta - (j-1)\frac{2\pi}{n}] \quad (3)$$

Where n is the number phase, a and b are coefficients found by transforming the series of Fourier [28].

The moment of phase j is expressed as follows,

$$T_j(\theta, i_j) = \frac{\psi_s}{f_j^2(\theta)}\frac{df_j(\theta)}{d\theta}\{1 - [1 + i_j f_j(\theta)]e^{-i_j f_j(\theta)}\} \quad (4)$$

Then, with the set of state vectors $\boldsymbol{x} = [x_1, x_2, x_3, x_4, x_5, x_6]^T = [\theta, \omega, i_1, i_2, i_3, i_4]^T$, the motor equation of state takes the form.

$$\dot{x}_1 = x_2 \quad (5)$$

$$\dot{x}_2 = \frac{1}{J}[T_1(\theta, x_3) + T_2(\theta, x_4) + T_3(\theta, x_5) + T_4(\theta, x_6) - T_l(x_1, x_2)]$$
$$= \frac{1}{J}\left[\begin{array}{l} \frac{\psi_s}{f_1^2(x_1)}\frac{\partial f_1(x_1)}{\partial x_1}\left\{1 - [1 + x_3 f_1(x_1)]e^{-x_3 f_1(x_1)}\right\} + \\ \frac{\psi_s}{f_2^2(x_1)}\frac{\partial f_2(x_1)}{\partial x_1}\left\{1 - [1 + x_4 f_2(x_1)]e^{-x_4 f_2(x_1)}\right\} + \\ \frac{\psi_s}{f_3^2(x_1)}\frac{\partial f_3(x_1)}{\partial x_1}\left\{1 - [1 + x_5 f_3(x_1)]e^{-x_5 f_3(x_1)}\right\} + \\ \frac{\psi_s}{f_4^2(x_1)}\frac{\partial f_4(x_1)}{\partial x_1}\left\{1 - [1 + x_6 f_4(x_1)]e^{-x_6 f_4(x_1)}\right\} \\ -Bx_2 - mgl\sin(x_1) \end{array}\right] \quad (6)$$

and $\dot{x}_3, \dot{x}_4, \dot{x}_5, \dot{x}_6$ are written in general as follows

$$\dot{x}_{j+2} = \left[-\psi_s e^{-x_{j+2} f_j(x_1)} f_j(x_1)\right]^{-1}\left[\begin{array}{l} \left(\psi_s e^{-x_{j+2} f_j(x_1)}\right)\left(x_{j+2}\frac{\partial f_j(x_1)}{\partial x_1}\right)x_2 \\ +Rx_{j+2} \end{array}\right] \quad (7)$$
$$+\left[\psi_s e^{-x_{j+2} f_j(x_1)} f_j(x_1)\right]^{-1} u_j$$

$$\frac{\partial f_j}{\partial x_1} = bN_r\cos\left(N_r x_1 - (j-1)\frac{2\pi}{4}\right) \qquad j = 1,2,3,4 \quad (8)$$

In equation (6), the load torque is determined, including the component Bx2 which is the damping coefficient against the motor shaft rotation, and the component $mgl\sin(x_1)$ is the mechanical load torque. For example, in the case of a motor shaft attached to a rod of length l, an object of mass m is attached to the other and of the rod [20].

Set

$$\begin{array}{l} g_j(\boldsymbol{x}) = \frac{1}{J}\left[\frac{\psi_s}{f_j^2(x_1)}\frac{\partial f_j(x_1)}{\partial x_1}\left\{1 - e^{-x_{j+2} f_j(x_1)}\right\}\right] \\ h_j(\boldsymbol{x}) = \frac{1}{J}\left[\frac{\psi_s}{f_j^2(x_1)}\frac{\partial f_j(x_1)}{\partial x_1}\left\{-f_j(x_1)e^{-x_{j+2} f_j(x_1)}\right\}\right] \end{array} \quad (9)$$

$$p_j(\boldsymbol{x}) = \left[-\psi_s e^{-x_{j+2} f_j(x_1)} f_j(x_1)\right]^{-1}\left[\begin{array}{l} Rx_{j+2} + \left(\psi_s e^{-x_{j+2} f_j(x_1)}\right) \\ \left(x_{j+2}\frac{\partial f_j(x_1)}{\partial x_1}\right)x_2 \end{array}\right] \quad (10)$$
$$q_j(\boldsymbol{x}) = \left[\psi_s e^{-x_{j+2} f_j(x_1)} f_j(x_1)\right]^{-1}$$

Where, j = 1, 2, 3, 4.
Equations (6) and (7) can be expressed as,

$$\dot{x}_2 = \sum_{j=1}^{4}\left[g_j(\boldsymbol{x}) + h_j(\boldsymbol{x})x_{j+2}\right] - \frac{B}{J}x_2 - \frac{mgl}{J}\sin(x_1) \quad (11)$$

$$\dot{x}_{j+2} = p_j(\boldsymbol{x}) + q_j(\boldsymbol{x})u_j \quad j = 1,2,3,4 \quad (12)$$

From (11) and (12), we get

$$\begin{aligned}\ddot{x}_2 &= \sum_{j=1}^{4}\left[\dot{g}_j(\boldsymbol{x}) + \dot{h}_j(\boldsymbol{x})x_{j+2} + h_j(\boldsymbol{x})\dot{x}_{j+2}\right] - \frac{B}{J}\dot{x}_2 \\ &-\frac{mgl}{J}\cos(x_1)\dot{x}_1 = \sum_{j=1}^{4}\begin{bmatrix}\dot{g}_j(\boldsymbol{x}) + \dot{h}_j(\boldsymbol{x})x_{j+2} + \\ +h_j(\boldsymbol{x})p_j(\boldsymbol{x}) + h_j(\boldsymbol{x})q_j(\boldsymbol{x})u_j\end{bmatrix} \\ &-\frac{B}{J}\dot{x}_2 - \frac{mgl}{J}\cos(x_1)\dot{x}_1\end{aligned} \quad (13)$$

For an SRM 8/6 with phase number 4, we obtain the following expression for each phase *j* (where *j* can take values 1, 2, 3, or 4)

$$u_j = k_j u \quad (14)$$

Where k_j is the phase transition key that can only take on the values of 0 or 1. Then, equation (13) becomes

$$\begin{aligned}\ddot{x}_2 =& \sum_{j=1}^{4}\left[\dot{g}_j(\boldsymbol{x}) + \dot{h}_j(\boldsymbol{x})x_{j+2} + h_j(\boldsymbol{x})p_j(\boldsymbol{x})\right] \\ &+\sum_{j=1}^{4}\left[h_j(\boldsymbol{x})q_j(\boldsymbol{x})k_j\right]u - \frac{B}{J}\dot{x}_2 - \frac{mgl}{J}\cos(x_1)\dot{x}_1\end{aligned} \quad (15)$$

Set

$$\begin{aligned}f(\boldsymbol{x}) =& \sum_{j=1}^{4}\left[\dot{g}_j(\boldsymbol{x}) + \dot{h}_j(\boldsymbol{x})x_{j+2} + h_j(\boldsymbol{x})p_j(\boldsymbol{x})\right] \\ &-\frac{B}{J}\dot{x}_2 - \frac{mgl}{J}\cos(x_1)\dot{x}_1\end{aligned} \quad (16)$$

and

$$g(\boldsymbol{x}) = \sum_{j=1}^{4}\left[h_j(\boldsymbol{x})q_j(\boldsymbol{x})k_j\right] \quad (17)$$

We obtain another form of equation (15) as follows

$$\ddot{x}_2 = f(\boldsymbol{x}) + g(\boldsymbol{x})u \quad (18)$$

In order to apply backstepping control to the SRM, Equation (18) must be rewritten in a strict feedback form. By defining new state variables $x_2 = z_1$, the SRM can be expressed in a different form, which is given

$$\begin{cases}\dot{z}_1 = z_2 \\ \dot{z}_2 = f(\boldsymbol{x}) + g(\boldsymbol{x})u\end{cases} \quad (19)$$

In the next section, we will design a backstepping slide mode controller for SRM based on (19).

3. Backstepping Sliding Mode Controller

In part 2, the nonlinear kinematics model of the SRM is presented in the form of a second-order back-propagation nonlinear model (19). According to the backstepping and sliding technique, the controller is designed in the following manner:

Let us denote

$$e_1 = z_1 - z_{1d} \quad (20)$$

Where z_{1d} is the setpoint of speed.

Taking the derivative of the equation e_2 with respect to time, we have

$$\dot{e}_1 = \dot{z}_1 - \dot{z}_{1d} = \dot{z}_1 - \dot{z}_{1d} \quad (21)$$

Put

$$e_2 = z_2 - \alpha \quad (22)$$

Within α is the virtual control signal, then we obtain

$$\dot{e}_1 = \dot{z}_1 - \dot{z}_{1d} = e_2 + \alpha - \dot{z}_{1d} \quad (23)$$

To obtain $e_1 \to 0$, we consider the Lyapunov function candidate of e_1 as follows

$$V_1 = \frac{1}{2}e_1^2 \quad (24)$$

Taking the derivative of the equation V_1 with respect to time, we have

$$\dot{V}_1 = e_1\dot{e}_1 = e_1\left(e_2 + \alpha - \dot{z}_{1d}\right) \quad (25)$$

For $\dot{V}_1 = -c_1e_1^2 + e_1e_2; c_1 > 0$ the virtual control signal to be

$$\alpha = -c_1e_1 + \dot{z}_{1d} \quad (26)$$

Definition of sliding surface is as follows

$$S = \mu e_1 + e_2; \mu > 0 \quad (27)$$

To ensure a stable closed system and tracking error of zero, we determine the sliding control signal $u(t)$ by using a positive-definite Lyapunov function (28)

$$V = V_1 + \frac{1}{2}S^2 \quad (28)$$

By taking the time derivative, we get:

$$\begin{aligned}\dot{V} &= -c_1e_1^2 + e_1e_2 + S\dot{S} = -c_1e_1^2 + e_1e_2 + S\left(\mu\dot{e}_1 + \dot{e}_2\right) \\ &= -c_1e_1^2 + e_1e_2 + S\left(\mu\dot{e}_1 + f(\boldsymbol{x}) + g(\boldsymbol{x})u - \dot{\alpha}\right) \\ &= -c_1e_1^2 - c_2e_2^2 - KS\,\mathrm{sgn}(S)\end{aligned} \quad (29)$$

if

$$e_1e_2 + c_2e_2^2 + S\left(K\,\mathrm{sgn}(S) + \mu\dot{e}_1 + f(\boldsymbol{x}) + g(\boldsymbol{x})u - \dot{\alpha}\right) = 0 \quad (30)$$

Then

$$\dot{V} = -c_1 e_1^2 - c_2 e_2^2 - KS\,\mathrm{sgn}(S) < 0$$

Therefore, we can guarantee the asymptotical stability of SRM by choosing the control signal as shown in equation (31)

$$u = -\frac{e_2\left(e_1 + c_2 e_2\right)}{Sg(\boldsymbol{x})} - \frac{K\,\mathrm{sgn}(S) + \mu\dot{e}_1 + f(\boldsymbol{x}) - \dot{\alpha}}{g(\boldsymbol{x})} \qquad (31)$$

The structure of the SRM with a backstepping sliding mode control algorithm is shown in Figure 2.

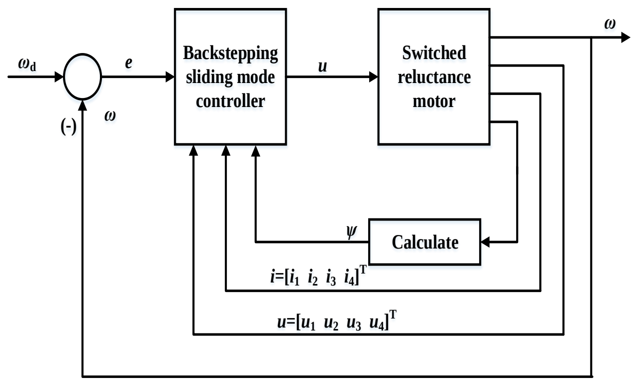

Fig. 2 System control backstepping sliding for SRM

4. The Simulation Results

The performance of a control system using a backstepping sliding mode controller (smc-btp) (as in Figure 2) was compared with that of a backstepping controller (btp) only under various scenarios.

Figure 4 shows the speed response of the two controllers at different speed ranges when the needle pulse control signal noise (as in Figure 3) affects the starting process at time 1s. The speed responses in low, medium and high-speed setpoints are shown in Figures 4a, 4b, and 4c. The quality of control during the start-up phase is presented in Table 1. The results indicate that the speed responses of the system with the proposed controller are more rapid and exhibit smaller overshoot. Particularly at a speed setpoint of 75 rad/s, the overshoot of the system with the backstepping controller is 73%, which is significantly larger than that of the system with the backstepping sliding mode controller.

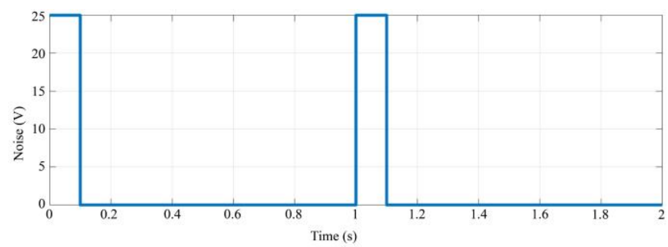

Fig. 3 Control signal noise

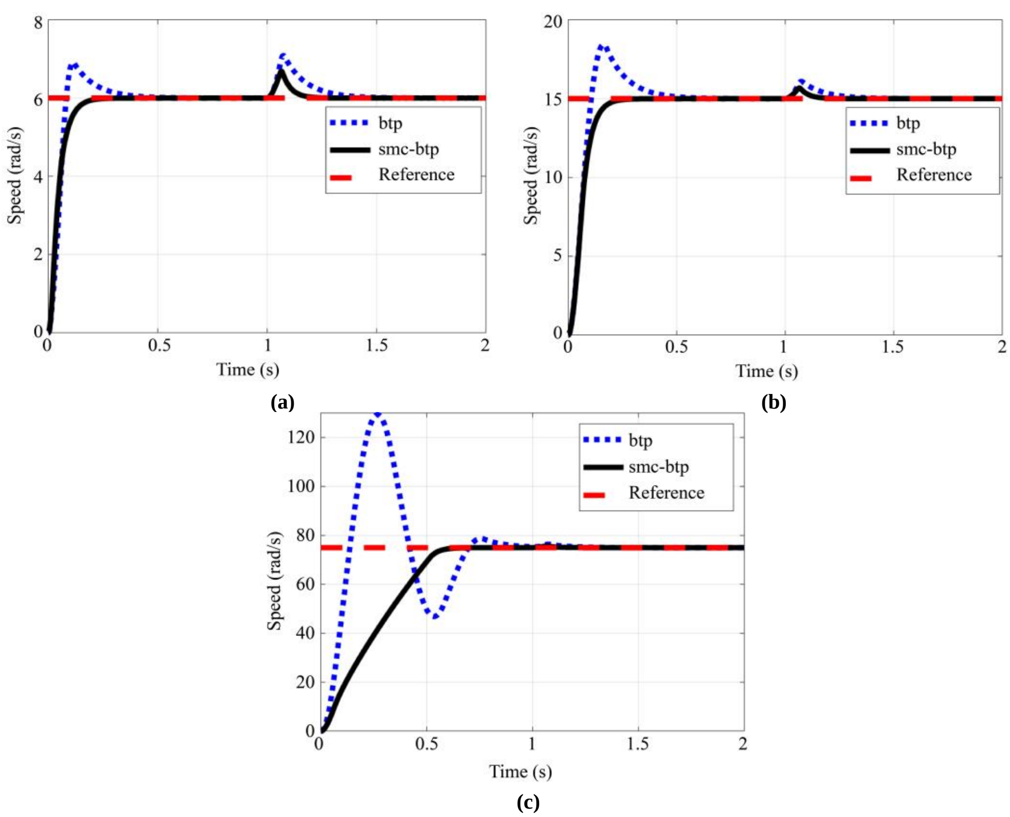

Fig. 4 Speed response of the two systems at different speed ranges

Table 1. Control the quality of the two systems at different setpoints

Setpoint of speed	**6 rad/s**		**15 rad/s**		**75 rad/s**	
Controller	smc-btp	btp	smc-btp	btp	smc-btp	btp
Overshoot	0%	13%	0%	20%	0%	73%
Settling time	0.2s	0.37s	0.25s	0.42s	0.53s	0.8s
Steady-state error	0	0	0	0	0	0

To assess the robustness and performance of the control systems under different operating conditions, we evaluated their speed response when subjected to signal noise and changes in the setpoint. Specifically, we examined the speed response of the two systems when the setpoint changed from 30 rad/s to 45 rad/s and when it changed from 90 rad/s down to 60 rad/s at time 1s. The speed response of the systems is presented in Figure 5, while Table 2 summarizes the control quality results for the different setpoints and scenarios.

The results provide insights into the effectiveness of the backstepping sliding mode controller (smc-btp) compared to the backstepping controller only (btp) in handling disturbances and changes in the setpoint. Notably, these results outperform the findings from [20], where the utilization of a nonlinear H-infinity controller led to an overshoot of roughly 20% and a settling time of approximately 2 seconds.

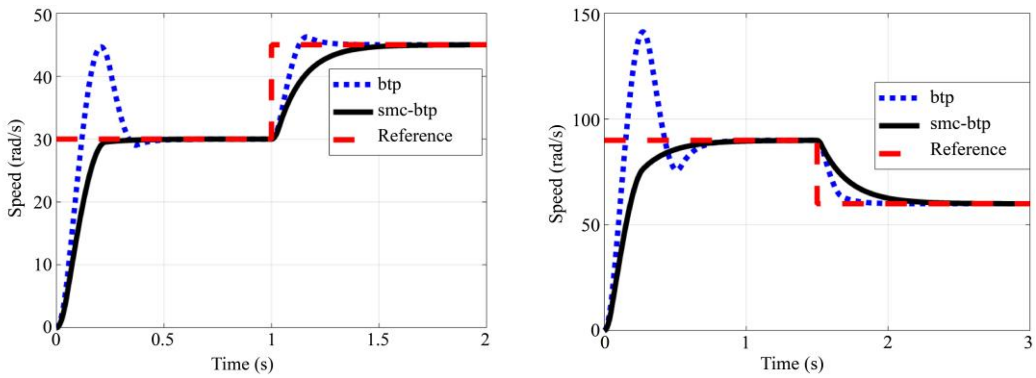

(a) **(b)**

Fig. 5 Speed response of the system when the setpoint changes

Table 2. Control the quality of the two systems when the setpoint changes

Setpoint changes	**From 30 rad/s to 45 rad/s**		**From 90 rad/s down 60 rad/s**	
Controller	smc-btp	btp	smc-btp	btp
Overshoot	0%	4%	0%	0%
Settling time	0.36s	0.3s	0.6s	0.27s
Steady-state error	0	0	0	0

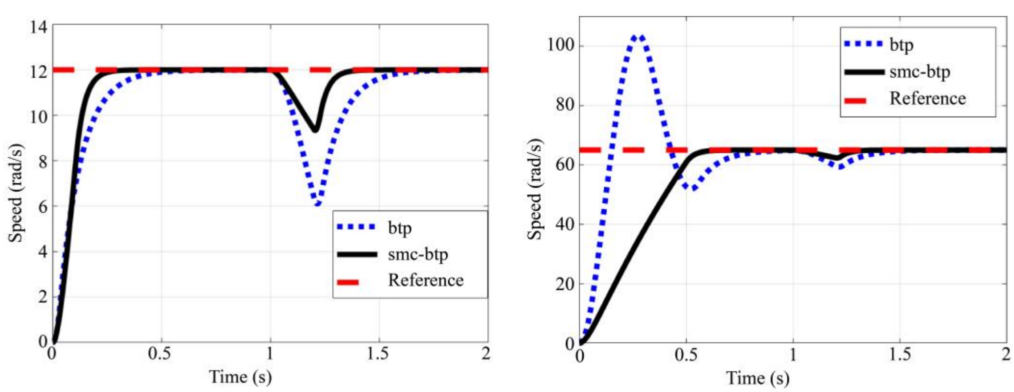

(a) **(b)**

Fig. 6 Speed response of the system under boost load conditions

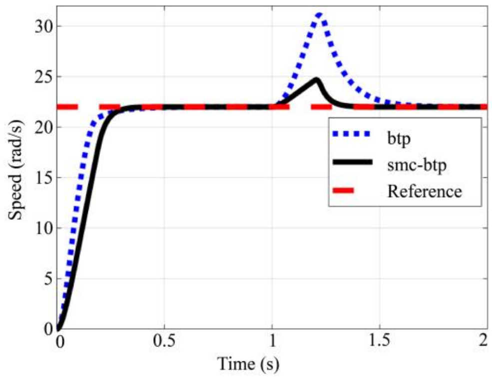

(a)

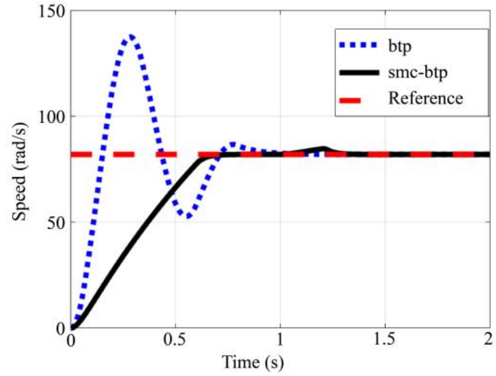

(b)

Fig. 7 Speed response of the system under offload conditions

Table 3. Control quality of the two systems under load changes

Load Changes	**Speed of 12 Rad/s and Load Increase at 1s**		**Speed of 22 Rad/s and Load Decrease at 1s**	
Controller	smc-btp	btp	smc-btp	btp
Overshoot	25%	67%	11%	41%
Settling Time	0.35s	0.6s	0.33s	0.55s
Steady-State Error	0	0	0	0

We further evaluated the performance of the control systems under load changes and signal noise during the start-up phase. Specifically, we analyzed the speed response of the two systems when subjected to boost load and offload conditions at time 1s. The speed responses of the systems are presented in Figures 6 and 7.

Figure 6 shows the speed response under boost load conditions, with Figures 6a and 6b representing speed levels of 12 rad/s and 65 rad/s, respectively. Figure 7 shows the speed response under offload conditions, with Figures 7a and 7b representing speed levels of 22 rad/s and 82 rad/s, respectively.

The control quality results for the different load conditions and scenarios are summarized in Table 3. These results provide insights into the ability of the backstepping sliding mode controller (smc-btp) and the backstepping controller only (btp) to handle load changes and signal noise during the start-up phase, which are critical for achieving stable and reliable system operation.

The results show that when the system is affected by load noise, the proposed controller quickly re-stabilizes the system with a shorter transient time and smaller overshoot compared to the backstepping algorithm.

5. Conclusion

In conclusion, this article proposes a backstepping sliding mode control algorithm for a combined nonlinear SRM that considers the nonlinear factors of both the motor and the inverter. The results demonstrate the feasibility of controlling the stability and tracking speed of the SRM drive system, as evidenced by the successful response to changes in speed setpoint and load disturbance. Furthermore, the backstepping sliding mode control algorithm achieves better control quality compared to both the backstepping control algorithm and the work presented in [20], with reduced overshoot and setting time. In the future, we will continue to research additional algorithms to further enhance the control quality of SRM drive systems under the influence of uncertain disturbances.

Acknowledgments

This research work was supported by the Hanoi University of Industry and Project Granted number 40-2022-RD/HĐ-ĐHCN.

References

[1] Diego F. Valencia et al., “Vision, Challenges, and Future Trends of Model Predictive Control in Switched Reluctance Motor Drives,” *IEEE Access*, vol. 9, pp. 69926-69937, 2021. [CrossRef] [Google Scholar] [Publisher Link]

[2] Phi Hoang Nha, and Dao Quang Thuy, “Improving the Characteristics of Switched Reluctance Motor,” *Automatic Control and System Engineering Journal*, vol. 16, no. 2, pp. 59-66, 2016. [Google Scholar] [Publisher Link]

[3] Yuanfeng Lan et al., “Switched Reluctance Motors and Drive Systems for Electric Vehicle Power Trains: State of the Art Analysis and Future Trends,” *Energies*, vol. 14, no. 8, pp. 1-29, 2021. [CrossRef] [Google Scholar] [Publisher Link]

[4] Peter Azer, Berker Bilgin, and Ali Emad, "Mutually Coupled Switched Reluctance Motor: Fundamentals, Control, Modeling, State of the Art Review and Future Trends," *IEEE Access*, vol. 7, pp. 100099-100112, 2019. [CrossRef] [Google Scholar] [Publisher Link]

[5] Jiancheng Song, Shichao Song, and Bingni Qu, "Application of an Adaptive PI Controller for a Switched Reluctance Motor Drive," *IEEE 2016 Annual Conference on Power Electronics*, Auckland, New Zealand, pp. 1-5, 2016. [CrossRef] [Google Scholar] [Publisher Link]

[6] Bogdan Fabianski, "Optimal Control of Switched Reluctance Motor Drive with Use of Simplified Nonlinear Reference Model," *7th IEEE International Conference on Mechatronics*, Prague, Czech Republic, pp. 1-8, 2016. [Google Scholar] [Publisher Link]

[7] Hsin-Ning Huang et al., "A Current Control Scheme with Back EMF Cancellation and Tracking Error Adapted Communication Shift for Switched Reluctance Motor Drive," *IEEE Transactions on Industrial Electronics*, vol. 69, no. 2, pp. 7381-7392, 2016. [CrossRef] [Google Scholar] [Publisher Link]

[8] Deepak Ronanki, and Sheldon S. Williamson, "Comparative Analysis of DITC and DTFC of Switched Reluctance Motor for EV Applications," *IEEE International Conference on Industrial Technology*, Ontario, Canada, pp. 509-514, 2017. [CrossRef] [Google Scholar] [Publisher Link]

[9] Mikhail Bychkov et al., "Torque Control of Switched Reluctance Drive in Generating Mode," *25th IEEE International Workshop on Electric Drives: Optimization in Control of Electric Drives*, Moscow, Russia, pp. 1-6, 2018. [CrossRef] [Google Scholar] [Publisher Link]

[10] Abdelmajid Berdai et al., "Similarity and Comparison of the Electrodynamics Characteristics of Switched Reluctance Motors SRM with those of Series DC Motors," *Engineering*, vol. 7, no. 1, pp. 36–45, 2017. [CrossRef] [Google Scholar] [Publisher Link]

[11] Akshay Nirgude et al., "Nonlinear Mathematical Modeling and Simulation of Switched Reluctance Motor," *IEEE International Conference on Power Electronics, Drives and Energy Systems*, pp. 1–6, 2016. [CrossRef] [Google Scholar] [Publisher Link]

[12] J. A. Makwana, P. Agarwal, and S. P. Srivastava, "Modeling and Simulation of Switched Reluctance Motor," *Lecture Notes Electrical Engineering*, vol. 442, pp. 545–558, 2018.

[13] Xiaodong Sun et al., "Direct Torque Control Based on a Fast Modeling Method for a Segmented-Rotor Switched Reluctance Motor in HEV Application," *IEEE Journal of Emerging and Selected Topics in Power Electronics*, vol. 9, no. 1, pp. 232-241, 2019. [CrossRef] [Google Scholar] [Publisher Link]

[14] Hady Abdelmaksoud, and Mohamed Zaky, "Design of an Adaptive Flux Observer for Sensorless Switched Reluctance Motors using Lyapunov Theory," *Advances in Electrical and Computer Engineering*, vol. 20, no. 2, pp. 123-130, 2020. [CrossRef] [Google Scholar] [Publisher Link]

[15] Berker Bilgin et al., "Making the Case for Switched Reluctance Motors for Propulsion Applications," *IEEE Transactions on Vehicular Technology*, vol. 69, no. 7, pp. 7172-7186, 2020. [CrossRef] [Google Scholar] [Publisher Link]

[16] Shuanghong Wang, Zihui Hu, and Xiupeng Cui, "Research on Novel Direct Instantaneous Torque Control Strategy for Switched Reluctance Motor," *IEEE Access*, vol. 8, pp. 66910-66916, 2020. [CrossRef] [Google Scholar] [Publisher Link]

[17] Gaoliang Fang et al., "Advance Control of Switched Reluctance Motors: A Review on Current Regulation, Torque Control and Vibration Suppression," *IEEE Access*, vol. 2, pp. 280-301, 2021. [CrossRef] [Google Scholar] [Publisher Link]

[18] Xinxin Shao et al., "Coupling Effect between Road Excitation and an In-Wheel Switched Reluctance Motor on Vehicle Ride Comfort and Active Suspension Control," *Journal of Sound and Vibration*, vol. 443, pp. 683-702, 2019. [CrossRef] [Google Scholar] [Publisher Link]

[19] Xiaodong Sun et al., "Direct Torque Control Based on a Fast Modeling Method for a Segmented Rotor Switched Reluctance Motor in HEV Application," *IEEE Journal of Emerging and Selected Topics in Power Electronics*, vol. 9, no. 1, pp. 232-241, 2019. [CrossRef] [Google Scholar] [Publisher Link]

[20] Gerasimos Rigatos, Pierluigi Siano, and Sul Ademi, "Nonlinear H-Infinity Control for Switched Reluctance Machines," *De Gruyter, Nonlinear Engineering*, vol. 9, no. 1, pp. 14–27, 2019. [CrossRef] [Google Scholar] [Publisher Link]

[21] Phi Hoang Nha et al., "Backstepping Control using Nonlinear State Observer for Switched Reluctance Motor," *Vietnam Journal of Science and Technology*, vol. 60, no. 3, pp. 554-568, 2022. [CrossRef] [Google Scholar] [Publisher Link]

[22] G. Dinesh, "A Modified Self Tuning Fuzzy Logic Controller for Brushless Direct Current Motor," *International Journal of Recent Engineering Science*, vol. 1, no. 4, pp. 22-27, 2014. [Publisher Link]

[23] M. T. Alrifai, J. H. Chow, and D. A. Torrey, "Backstepping Nonlinear Speed Controller for Switched-Reluctance Motors," *IEE Proceedings - Electric Power Applications*, vol. 150, no. 2, pp. 193–200, 2003. [CrossRef] [Google Scholar] [Publisher Link]

[24] R. Surendiran, "Modified Field-Oriented Control-Based Sensorless Speed Control for BLDC Motor via Elephant Herding Optimization," *DS Journal of Digital Science and Technology*, vol. 1, no. 2, pp. 11-17, 2022. [CrossRef] [Google Scholar] [Publisher Link]

[25] C. H. Lin, "Adaptive Nonlinear Backstepping Control using Mended Recurrent Romanovski Polynomials Neural Network and Mended Particle Swarm Optimization for Switched Reluctance Motor Drive System," *Transactions of the Institute of Measurement and Control*, vol. 41, no. 14, pp. 4114–4128, 2019. [CrossRef] [Google Scholar] [Publisher Link]

[26] Kingshuk Chowdhury et al., "RC Servo and Stepper Motor Control using Verilog HDL," *SSRG International Journal of VLSI & Signal Processing*, vol. 2, no. 3, pp. 18-24, 2015. [CrossRef] [Google Scholar] [Publisher Link]

[27] Chih Hong Lin, and Jung Chu Ting, "Novel Nonlinear Backstepping Control of Synchronous Reluctance Motor Drive System for Position Tracking of Periodic Reference Input Torque Ripple Consideration," *International Journal of Control, Automation and Systems*, vol. 17, no. 1, pp. 1-17, 2019. [CrossRef] [Google Scholar] [Publisher Link]

[28] Hala Hannoun, Mickael Hilairet, and Claude Marchand, "High-Performance Current Control of a Switched Reluctance Machine Based on a Gain-Scheduling PI Controller," *Control Engineering Practice*, vol. 19, no. 11, pp. 1377-1386, 2011. [CrossRef] [Google Scholar] [Publisher Link]

Appendix 1. SRM and Simulation Parameters

Number of rotor poles 6	$J=6.8x10^3$ kg/m^2
Number of stator poles 8	$a=1.5x10^3$ H
Number of phases 4	$b=1.364x10^3$ H
Power 5.5 HP	B=0.2
Peak current 9A	l=2 m
Stator winding resistance 0.72 Ω	$c_1=2$
Aligned phase inductance 130 mH	$c_2=0.1$
Unaligned phase inductance 12 mH	T=0.025